

Supporting Information

Layered Na_{1-x}Ni_yFe_{1-y}O₂ Double Oxide Oxygen Evolution Reaction Electrocatalyst for Highly Efficient Water-splitting†

*Baicheng Weng, Fenghua Xu, Changlei Wang, Weiwei Meng, Corey R. Grice, and Yanfa Yan**

* Correspondence and requests for materials should be addressed to Y.F.Y. (email: yanfa.yan@utoledo.edu).

Experimental

Methods

Material synthesis: Ni(NO₃)₂ (or Co(NO₃)₂) and Fe(NO₃)₂ powders were mixed at stoichiometric ratios and then calcinated at 550 °C for 2 h in Air at a heating rate of 2 °C min⁻¹. After cooling down to room temperature, as-obtained NiFeO_x powders were ground with Na₂O₂ at stoichiometric ratios and then calcinated at 650 °C for 12 h in Air at a heating rate of 10 °C min⁻¹. Na extractions were carried out in a 1 M I₂ acetonitrile solution for various durations at room temperature. After Na extraction, the powders were filtered and washed with ethanol and dried at 80 °C before further usage. NiP electrocatalyst was prepared according to reported literature.^{S1, S2} Ruthenium oxide (RuO₂, were synthesized according to the literatures.^{S3, S4} Cyclic voltammetry was performed at the potential region from 0.06 to 0.96 V (vs Ag/AgCl/KCl) with a scan rate of 50 mV s⁻¹. After electrodeposition, the obtained films were annealed at 200°C for 3 h in air. The solution

was 0.45 g RuCl₃, 2.98 g KCl and 0.01 M HCl. The as-prepared RuO₂ has the grain size of 500 nm.

Perovskite solar cell fabrication: FTO glass (15 Ω □⁻¹) and ITO/PET (45 Ω □⁻¹) substrates were cleaned prior to Plasmon enhanced atomic layer deposition (PEALD) of SnO₂. Tetrakis(dimethylamino)-tin(IV) was used as the Sn precursor and pure O₂ was used as the oxidizer. Ar was used as the carrier gas with a flow rate of 15 sccm. PEALD SnO₂ was deposited at 100 °C with an Ensure Scientific Group AutoALD-PE V2.0 equipped with a plasma generator. The TDMA-Sn precursor was held at 75 °C. The resulting deposition rate is about 1.7 Å per cycle as determined by spectroscopic ellipsometry. A 45% by weight precursor solution was prepared with lead iodide and methylammonium iodide (MAI) (molar ratio = 1 : 1) in *N,N*-dimethylformamide (DMF) and dimethyl sulfoxide (DMSO) (volume ratio = 9 : 1). A small amount of lead thiocyanate was added into the precursor solution as an additive.^{S5} The solution was stirred for 12 hours on a 60 °C hot plate before deposition. The C₆₀-SAM (4 mg mL⁻¹ in chlorobenzene) was then deposited onto the SnO₂ ESL by a spin coating method. The perovskite precursor solution was spin-coated on the C₆₀-SAM/SnO₂ ESLs first at 500 rpm for 3 s and then at 4000 rpm for 60 s. Diethyl ether, as the anti-solvent agent, was then drop-cast on the substrate. After spin coating, the perovskite film was annealed at 65 °C for 2 minutes and then at 100 °C for 5 minutes. All of these processes were carried out in a N₂ filled glove box. Spiro-OMeTAD was used as the HSL and deposited on the perovskite film at 2000 rpm for 60 seconds. The Spiro-OMeTAD solution was prepared by dissolving 72.3 mg Spiro-OMeTAD in 1 mL chlorobenzene with 28 μL 4-*tert*-butylpyridine and 18 μL Li-bis(trifluoromethanesulfonyl)imide (520 mg mL⁻¹ in acetonitrile). A layer of 80 nm gold

(Au) was then deposited on the top of Spiro-OMeTAD using thermal evaporation. The working area of the devices was 0.25 cm^2 as defined by a shadow mask during the Au evaporation. Two single perovskite solar cells were assembled as depicted schematically in Figure 5d. The cathode of one cell was directly soldered to the anode of the second cell to wire them together in a series connection. Copper wires were then soldered to the other contacts to make a connection to the water splitting electrodes.

Materials characterizations: The structure and phase of the synthesized materials were examined by X-ray diffraction (XRD) (Ultima III, Rigaku, Japan) and Raman (Bruker FT Raman Spectrometer with laser wavelength of 532 nm). The morphology of the films was characterized by a scanning electron microscope (SEM) (Hitachi S-4800, Hitachi, Japan) and scanning transmission electron microscope (STEM) (Hitachi HD-2300A, Hitachi, Japan). Elemental compositions were measured by energy-dispersive X-ray spectroscopy (EDX) (Oxford Instruments, UK) and inductively coupled plasma mass spectrometry (ICP-MS, Thermo Scientific XSeries 2 ICPMS, USA). For perovskite solar cells, current density–voltage (J – V) curves were obtained under standard AM 1.5 G illumination using a solar simulator (PV Measurements, Inc) equipped with a 450 W xenon lamp with an output intensity of 100 mW cm^{-2} calibrated with a reference Si cell at the measurement location. The light intensity was later adjusted between 0.5 and 100 mW cm^{-2} using neutral density filters.

Electrochemical characterizations: The electrochemical measurements were performed using a Solartron potentiostat (Solartron, USA), with a platinum foil and an Ag/AgCl electrode used as the counter and reference electrodes, respectively. The HER and OER characterization were carried out on a glassy carbon rotating disk electrode at a

rate of 1,000 r.p.m. The obtained powders were dispersed in ethanol and dropped on the tip of glassy carbon electrode and then dried in ambient air. For preparing water splitting electrodes, 1.5 mm thick nickel foam (>99.5%, 1.5 mm, MTI Corporation, USA) was compressed to ~1 mm using a hydraulic press, which helped increase the adhesion of the catalysts and to define the geometric area. The as-prepared catalysts and RuO₂ and IrO₂ are dropped on the surface of Ni foam and dried in Air. The loading amount of catalysts is 0.13 mg cm⁻². The potentials were displayed versus reversible hydrogen electrode (RHE) by: $E_{(RHE)} = E_{(Ag/AgCl)} + 0.197 + 0.0591 \times \text{pH}$. All the linear sweep voltammetry measurements were carried out at a scan rate of 5 mV·s⁻¹. All of the electrochemical measurements were iR-compensated. The electrolyte was 1 M KOH (semiconductor grade, 99.99%, and 18.2 MΩ cm⁻¹ DI water), which was deaerated with high-purity argon prior to and throughout all the measurements. The electrochemical double layer capacitances (C_{dl}) of the as-synthesized materials were measured from double-layer charging curves using cyclic voltammograms (CVs) in a potential range of 0-0.05 V vs. SCE. Working electrodes were scanned for several potential cycles until the signals were stabilized, and then the CV data were collected. Then, the capacitive currents were plotted as a function of CV scan rate. The stability test was performed using the controlled potential electrolysis method. The H₂ and O₂ evolution was conducted under potentiostatic mode at each potential. Gaseous products from the outlet of the electrode compartment were vented directly into the gas-sampling loop of the gas chromatograph (GC, InficonMicro 3000 GC), with a GC run initiated every 10 min. The gas concentration was averaged over three measurements. Faradaic efficiency was calculated according to that 96485 C of electrons can generate 0.5 mol of H₂ and 0.25 mol of O₂. The current of the water splitting cell was recorded by

chronoamperometry without applying an external bias for different time periods under chopped AM 1.5G illumination. For the device in Figure 5, the geometric catalyst electrode area was $\sim 1 \text{ cm}^2$.

Supporting Figures

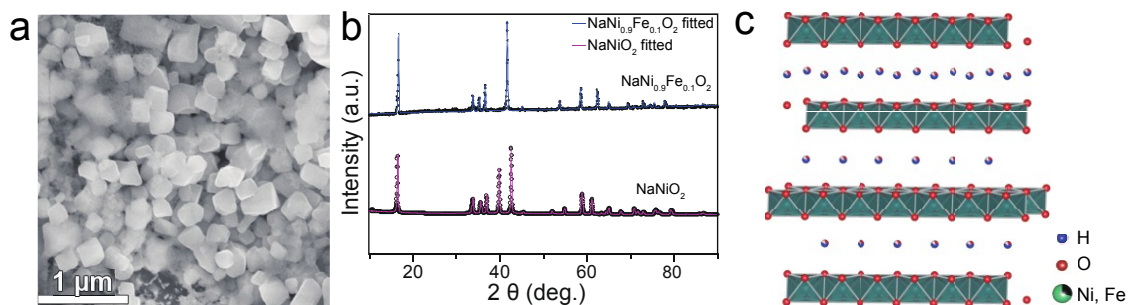


Fig. S1. (a) SEM image of obtained $\text{NaNi}_{0.9}\text{Fe}_{0.1}\text{O}_2$ powder. (b) Rietveld refined XRD patterns of $\text{NaNi}_{0.9}\text{Fe}_{0.1}\text{O}_2$ and $\text{NaCo}_{0.8}\text{Fe}_{0.2}\text{O}_2$ samples. (c) Crystal structure of NiFe-LDH

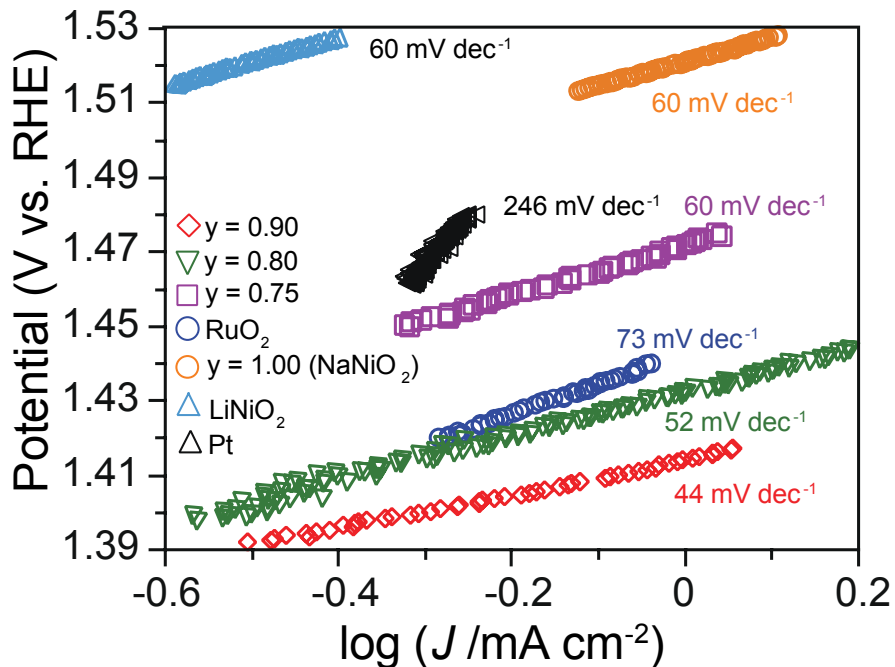


Fig. S2. Tafel plot of NaNiO_2 , LiNiO_2 and LiCoO_2 in 1 M KOH solution.

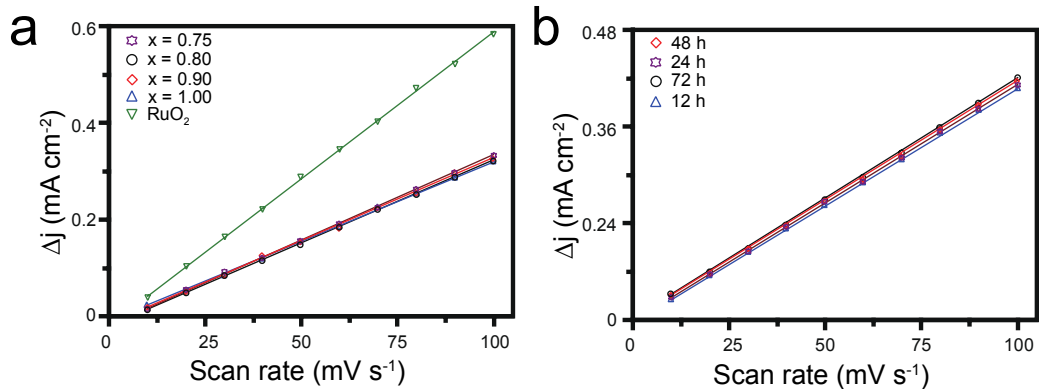


Fig. S3. Double-layer capacitance measurements for determining electrochemically-active surface area (ECSA) of $\text{NaNi}_y\text{Fe}_{1-y}\text{O}_2$ samples (a) and Na extracted $\text{NaNi}_{0.9}\text{Fe}_{0.1}\text{O}_2$ samples with various durations (b). The anodic charging currents plotted as a function of scan rate. The working electrode was held at each potential vertex for 10 s before the beginning the next sweep.

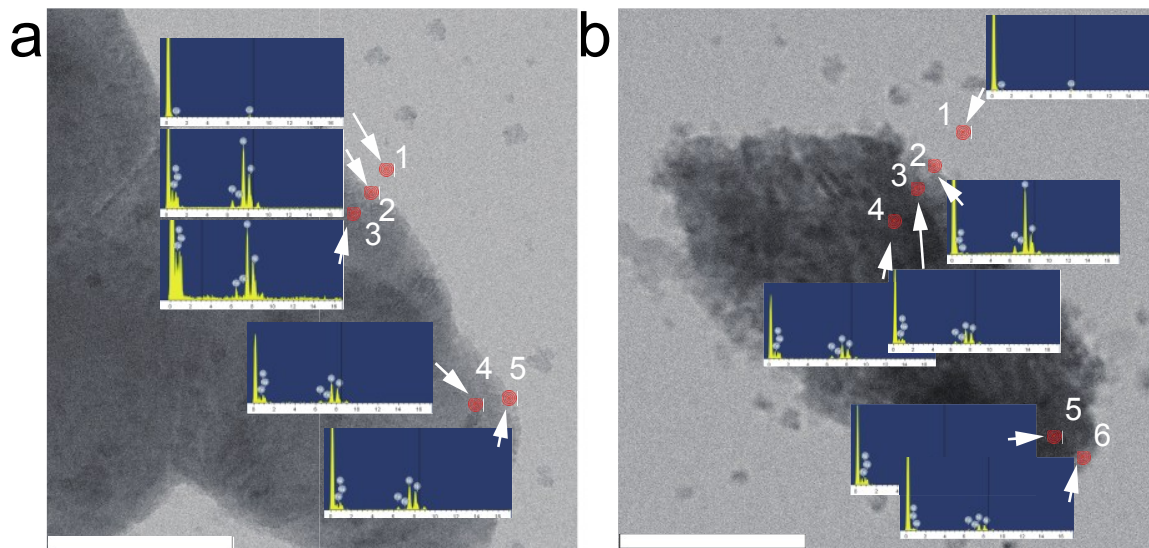


Fig. S4. TEM and EDS analysis of $\text{NaNi}_{0.9}\text{Fe}_{0.1}\text{O}_2$ surface before (a) and after cycling testing (b). Scale bar 200 nm.

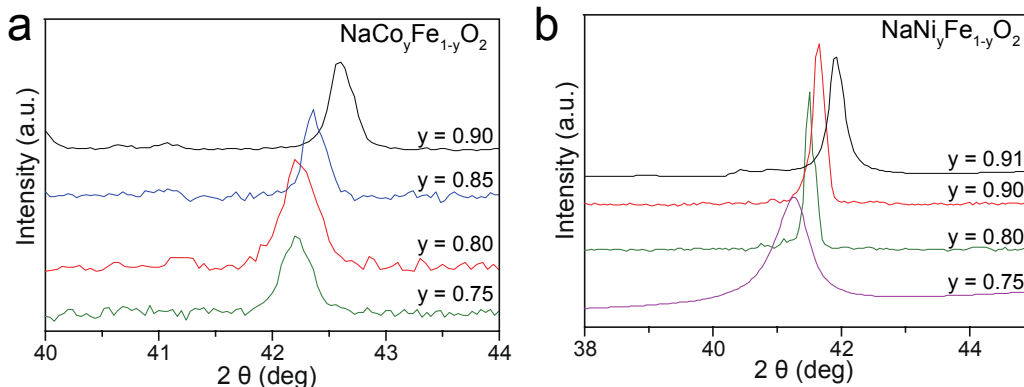


Fig. S5. (a) Magnified XRD patterns shown in Fig. 1a showing the shift of the main peaks. (b) Magnified PXRD patterns shown in Fig. S2, showing the shift of the main peaks as a function of y .

Rietveld refined XRD patterns show that $\text{NaCo}_y\text{Fe}_{1-y}\text{O}_2$ and $\text{NaNi}_y\text{Fe}_{1-y}\text{O}_2$ samples have the O3-type crystal structure. Similar to $\text{NaNi}_y\text{Fe}_{1-y}\text{O}_2$, with increased y value, the unit cell volume decreases due to the smaller ionic radius of Co than Fe, and the larger electronegativity of Co. The corresponding PXRD patterns show peaks shift to higher angles with the increase of y value (Fig. S2b). The $\text{NaNi}_y\text{Fe}_{1-y}\text{O}_2$ samples have the similar trend, but has smaller MeO_6^- units due to the even larger electronegativity of Ni atom than Co.

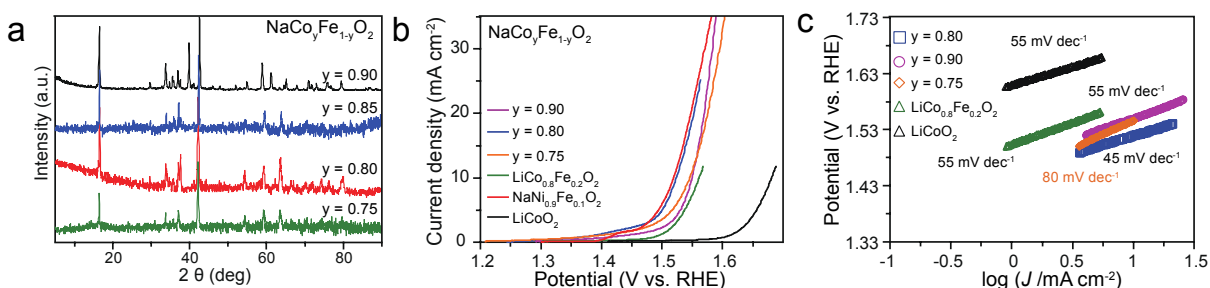


Fig. S6. (a) XRD patterns of $\text{NaCo}_y\text{Fe}_{1-y}\text{O}_2$ samples. (b) OER polarization curves of $\text{NaCo}_y\text{Fe}_{1-y}\text{O}_2$ with various y values in a 1 M KOH solution. (c) Corresponding Tafel plots of (b).

$\text{NaCo}_y\text{Fe}_{1-y}\text{O}_2$ samples with other compositions ($y = 0.9$ and 0.75) also show high activity, even though not as high as that of the $\text{NaCo}_{0.8}\text{Fe}_{0.2}\text{O}_2$ sample. For instance, the onset

potential for $\text{NaCo}_{0.9}\text{Fe}_{0.1}\text{O}_2$ is 1.35 V vs. RHE. The potentials at 10 mA cm^{-2} for $\text{NaCo}_{0.9}\text{Fe}_{0.1}\text{O}_2$ and $\text{NaCo}_{0.75}\text{Fe}_{0.25}\text{O}_2$ are 1.55 V and 1.54 V vs. RHE, respectively, and the corresponding Tafel slopes are 55 and 80 mV dec^{-1} , respectively. $\text{NaCo}_{0.8}\text{Fe}_{0.2}\text{O}_2$ and $\text{NaNi}_{0.9}\text{Fe}_{0.1}\text{O}_2$ samples exhibit higher OER activities than $\text{LiCo}_{0.8}\text{Fe}_{0.2}\text{O}_2$ and LiCoO_2 samples. $\text{LiCo}_{0.8}\text{Fe}_{0.2}\text{O}_2$ and LiCoO_2 show onset potentials of 1.45 V and 1.6 V vs. RHE, potentials of 1.56 V and 1.68 V vs. RHE at 10 mA cm^{-2} , and both Tafel slopes of 60 mV dec^{-1} , respectively.

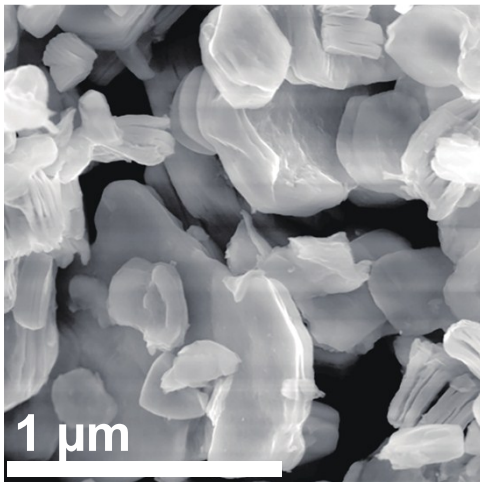


Fig. S7. SEM images of $\text{Na}_{0.08}\text{Ni}_{0.9}\text{Fe}_{0.1}\text{O}_2$ sample (48 h of Na extraction).

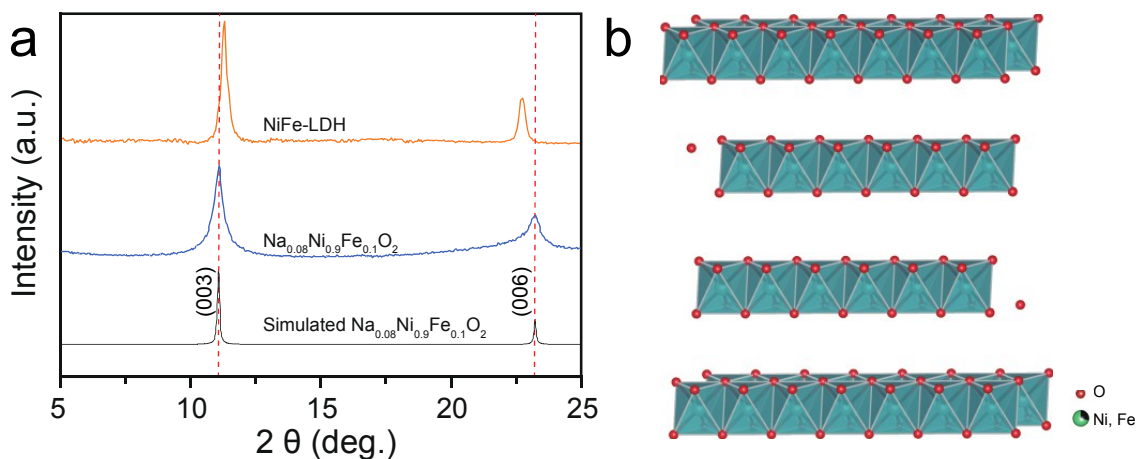


Fig. S8. (a) Comparison of XRD patterns of NiFe-LDH, $\text{Na}_{0.08}\text{Ni}_{0.9}\text{Fe}_{0.1}\text{O}_2$ and its simulated XRD pattern. (b) Corresponding crystal structure of $\text{Na}_{0.08}\text{Ni}_{0.9}\text{Fe}_{0.1}\text{O}_2$.

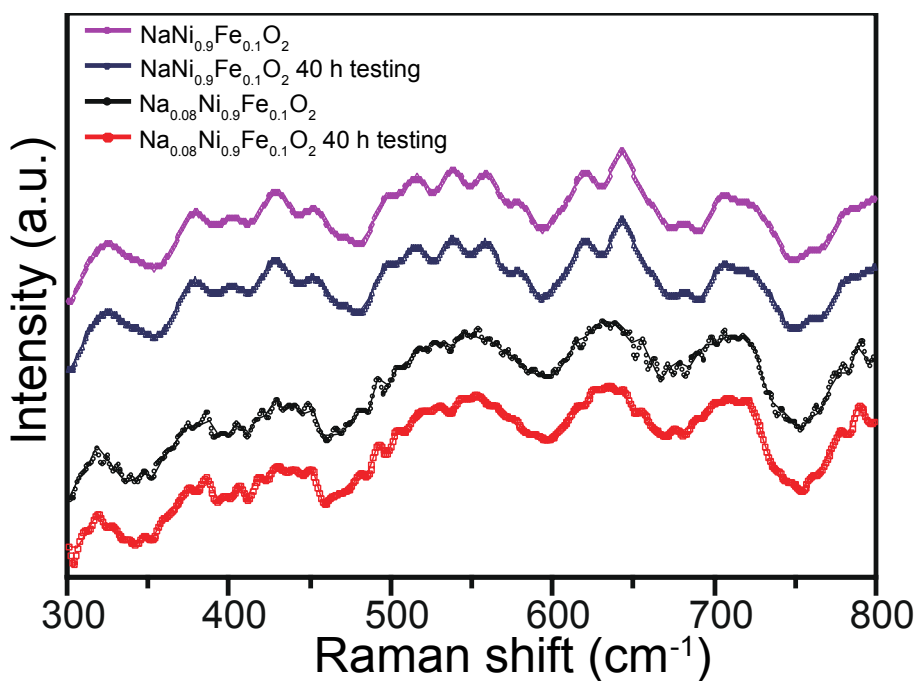


Fig. S9. Raman spectra of $\text{NaNi}_{0.9}\text{Fe}_{0.1}\text{O}_2$ sample (purple and navy lines) and $\text{Na}_{0.08}\text{Ni}_{0.9}\text{Fe}_{0.1}\text{O}_2$ samples (black and red lines) before and after 40 h durability test.

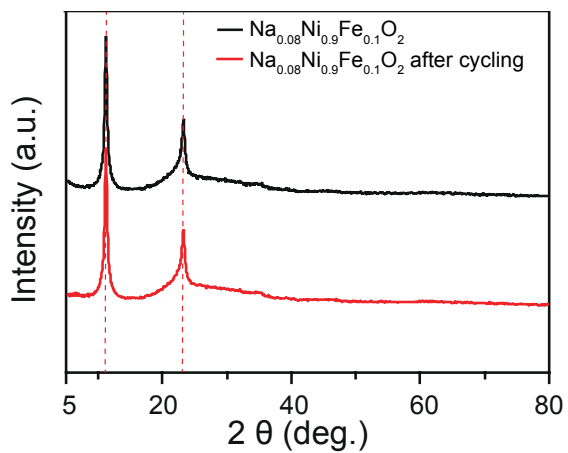


Fig. S10. XRD patterns of $\text{Na}_{0.08}\text{Ni}_{0.9}\text{Fe}_{0.1}\text{O}_2$ sample before and after durability test.

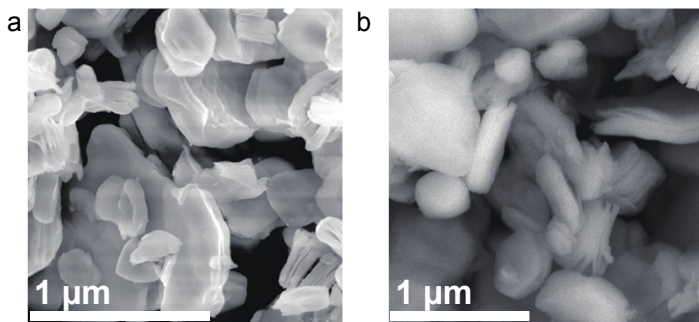


Fig. S11. SEM images of $\text{Na}_{0.08}\text{Ni}_{0.9}\text{Fe}_{0.1}\text{O}_2$ sample before (a) and after (b) durability test.

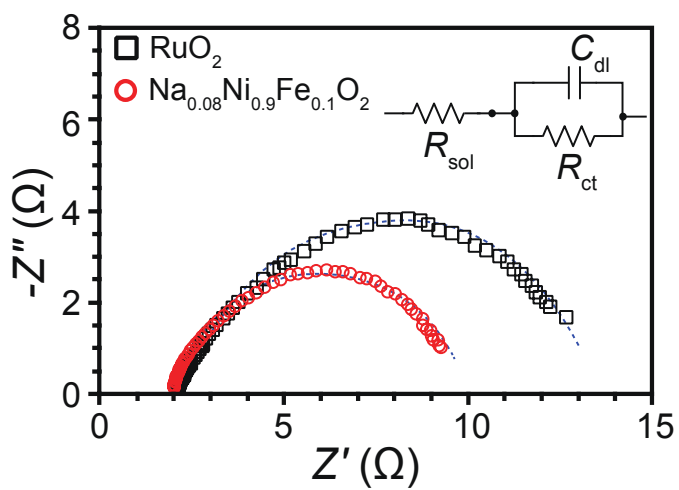


Fig. S12. EIS curves of RuO_2 and $\text{Na}_{0.08}\text{Ni}_{0.9}\text{Fe}_{0.1}\text{O}_2$ electrodes. Inset circuit model: R_s , resistance of

solution; R_{ct} charge transfer resistance; C_{dl} , double-layer capacitance. Dash lines are the fitting curves according to the inserted circuit model.

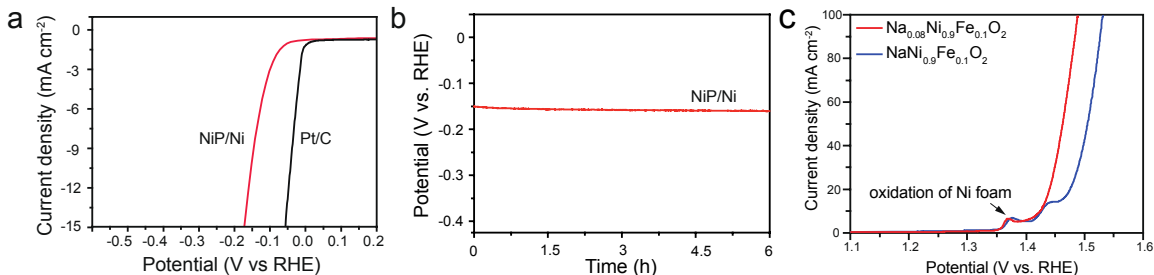


Fig. S13. (a) HER polarization curves of NiP on Ni foam in 1.0 M KOH solution. (b) Durability test for NiP on Ni foam at -10 mA cm^{-2} in 1.0 M KOH solution. (c) OER polarization curves of $\text{NaNi}_{0.9}\text{Fe}_{0.1}\text{O}_2$ and $\text{Na}_{0.08}\text{Ni}_{0.9}\text{Fe}_{0.1}\text{O}_2$ samples deposited on Ni foam in 1.0 M KOH.

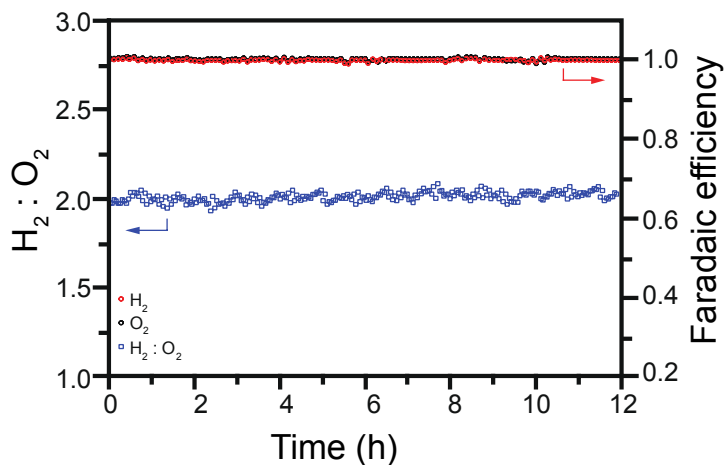


Fig. S14. Gas ratio and Faradaic efficiency from gas chromatography measurement of evolved H_2 and O_2 from $\text{Na}_{0.08}\text{Ni}_{0.9}\text{Fe}_{0.1}\text{O}_2/\text{Ni}_3\text{P}_2$ samples in two-electrode system.

Table S1 Comparison of OER performance for $\text{Na}_x\text{Ni}_y\text{Fe}_{1-y}\text{O}_2$ and RuO_2 .

Samples	Potential (V vs. RHE) at 10 mA cm ⁻²	Tafel slope (mV dec ⁻¹)	C_{dl} (mF cm ⁻²)	Current density @ $\eta = 0.35$ V	$ j_s $ (mA cm ⁻²) (ECSA) @ $\eta = 0.35$ V
NaNiO_2	1.56	60	1.19	10.3	0.35
$\text{NaNi}_{0.9}\text{Fe}_{0.1}\text{O}_2$	1.52	44	1.20	34.6	1.15
$\text{NaNi}_{0.8}\text{Fe}_{0.2}\text{O}_2$	1.55	52	1.20	25.2	0.84
$\text{NaNi}_{0.75}\text{Fe}_{0.25}\text{O}_2$	1.56	60	1.21	18.6	0.61
$\text{Na}_{0.41}\text{Ni}_{0.9}\text{Fe}_{0.1}\text{O}_2$	1.50	60	1.56	35.2	0.90
$\text{Na}_{0.24}\text{Ni}_{0.9}\text{Fe}_{0.1}\text{O}_2$	1.49	43	1.57	40.3	1.03
$\text{Na}_{0.08}\text{Ni}_{0.9}\text{Fe}_{0.1}\text{O}_2$	1.49	40	1.57	62.1	1.58
$\text{Na}_{0.01}\text{Ni}_{0.9}\text{Fe}_{0.1}\text{O}_2$	1.50	53	1.59	45.5	1.14
RuO_2	1.58	73	2.01	20.2	0.41
RuO_2^*	1.58	55	N/A	17.5 – 32.4	0.49

* *Nat. Commun.* **2015**, 6, 8106; *J. Am. Chem. Soc.* **2015**, 137, 4347–4357

Table S2 Comparison of OER performance for $\text{NaNi}_{0.9}\text{Fe}_{0.1}\text{O}_2$, $\text{NaCo}_{0.8}\text{Fe}_{0.2}\text{O}_2$, $\text{Na}_{0.08}\text{Ni}_{0.9}\text{Fe}_{0.1}\text{O}_2$, and other reported electrocatalysts.

Samples	Potential (V vs. RHE) at 10 mA cm ⁻²	Tafel slope (mV dec ⁻¹)	Loading amount (mg cm ⁻²)	References
$\text{Na}_{0.08}\text{Ni}_{0.9}\text{Fe}_{0.1}\text{O}_2$	1.49	40	0.130	<i>This work</i>
$\text{NaNi}_{0.9}\text{Fe}_{0.1}\text{O}_2$	1.52	44	0.130	<i>This work</i>
$\text{NaCo}_{0.8}\text{Fe}_{0.2}\text{O}_2$	1.56	45	0.130	<i>This work</i>
RuO_2 (as reference)	1.58	73	0.130	<i>This work</i>
RuO_2	1.58	55	0.025	<i>Nat. Commun.</i> 2015 , 6, 8106
LT-LiCoO ₂	1.66	48	0.32	<i>Energy Environ. Sci.</i> 2016 , 9, 184-192
NiD-PCC	1.59	98	N/A	<i>Energy Environ. Sci.</i> 2016 , DOI: 10.1039/C6EE01930G

Ni ₃ Se ₂	1.54	97	0.217	<i>Energy Environ. Sci.</i> 2016 , 9, 1771--1782
FeNi@NC	1.51	70	0.32	<i>Energy Environ. Sci.</i> 2016 , 9, 123--129
Ni-P nanoplates	1.53	64	0.20	<i>Energy Environ. Sci.</i> 2016 , 9, 1246--1250
De-LCoP@5.1 V	1.654	73	0.50	<i>Energy Environ. Sci.</i> 2015 , 8, 1719--1724
LT-LiCoO ₂	1.61	52	0.25	<i>Nat. Commun.</i> 2014 , 5, 3949
LiCo _{0.8} Fe _{0.2} O ₂	1.58	50	0.232	<i>Adv. Mater.</i> 2015 , 27, 7150–7155
LiNi _{0.8} Al _{0.2} O ₂	1.58	44	0.051	<i>Adv. Mater.</i> 2015 , 27, 6063–6067
NiV-LDH	1.55	64	0.143	<i>Nat. Commun.</i> 2016 , 7, 11981
NiFe-LDH (exfoliated 2-D nanosheets)	1.53	82	0.25	<i>ACS Nano</i> 2015 , 9, 1977-1984
CoMn-LDH (2-D nanosheets)	1.53	43	0.222	<i>J. Am. Chem. Soc.</i> 2014 , 136, 16481-16484
NiCo-LDH	1.62	59	0.07	<i>Nat. Commun.</i> 2014 , 5, 4477
NiFe*	1.65	N/A	N/A	<i>Nat. Commun.</i> 2015 , 6, 6616
Co ₃ O ₄ /rm-GO	1.54	67	0.17	<i>Nat. Mater.</i> 2011 , 10, 780
N-doped graphene-CoO	1.57	71	N/A	<i>Energy Environ. Sci.</i> 2014 , 7, 609

* on glassy carbon

Table S3 ICP-MS analysis of NaNi_{0.9}Fe_{0.1}O₂ samples before and after chronopotentiometric test.

Samples	ICP-MS analysis			Composition
	Metal ions concentrations (ppm)			
	Na	Ni	Fe	
Before cycling	106.36	95.92	10.63	Na _{0.998} Ni _{0.9} Fe _{0.1} O ₂
After cycling	99.30	89.68	9.94	Na _{0.996} Ni _{0.9} Fe _{0.1} O ₂

Table S4 EDS analysis of $\text{NaNi}_{0.9}\text{Fe}_{0.1}\text{O}_2$ samples before and after chronopotentiometric test in Fig. S4.

	Sites	Atomic ratios		
		Na	Ni	Fe
Before cycling	1	0.00	0.00	0.00
	2	49.19	45.73	5.08
	3	48.79	46.27	4.94
	4	49.35	45.67	4.98
	5	48.78	45.6	5.62
After cycling	1	0.00	0.00	0.00
	2	36.41	57.16	6.43
	3	43.06	51.43	5.51
	4	49.91	44.98	5.11
	5	49.23	45.37	5.40
	6	24.26	68.21	7.63

Table S5 ICP-MS and EDS analysis of $\text{Na}_{0.08}\text{Ni}_{0.9}\text{Fe}_{0.1}\text{O}_2$ samples before and after chronopotentiometric test.

Samples	ICP-MS analysis			EDS analysis			Composition
	Metal ions concentrations (ppm)			Atomic ratios			
	Na	Ni	Fe	Na	Ni	Fe	
Before cycling	7.91	88.94	9.86	7.42	83.33	9.26	$\text{Na}_{0.08}\text{Ni}_{0.9}\text{Fe}_{0.1}\text{O}_2$
After cycling	8.90	100.15	11.10	7.51	82.28	9.21	$\text{Na}_{0.08}\text{Ni}_{0.9}\text{Fe}_{0.1}\text{O}_2$

References

- [S1]B. Weng, W. Wei, Yiliguma, H. Wu, A. M. Alenizi and G. Zheng. *J. Mater. Chem. A*, 2016, **4**, 15353.

- [S2] S. Meng, H. Liu, J. Qu and J. Li. *Adv. Funct. Mater.* 2016, **6**, 1600087.
- [S3] C. C. L. McCrory, S. Jung, I. M. Ferrer, S. M. Chatman, J. C. Peters and T. F. Jaramillo, *J. Am. Chem. Soc.*, 2015, **137**, 4347.
- [S4] E. Tsuji, A. Imanishi, K. I. Fukui and Y. Nakato, *Electrochim. Acta* 2011, **56**, 2009.
- [S5] C. Wang, D. Zhao, C. R. Grice, W. Liao, Y. Yu, A. Cimaroli, N. Shrestha, P. J. Roland, J. Chen Z. Yu, P. Liu, N. Cheng, R. J. Ellingson, X. Zhao and Y. Yan. *J. Mater. Chem. A*, 2016, **4**, 12080